



Cite this: DOI: 10.1039/c6nj00440g

# Hydrothermal synthesis of two supramolecular inorganic–organic hybrid phosphomolybdates based on Ni(II) and Co(II) ions: structural diversity and heterogeneous catalytic activities†

Luna Paul,<sup>a</sup> Malay Dolai,<sup>a</sup> Anangamohan Panja<sup>b</sup> and Mahammad Ali\*<sup>a</sup>

Two new hybrid compounds based on phosphomolybdates, namely (NHEPH<sub>2</sub>)<sub>5</sub>[Ni<sup>II</sup>(P<sub>4</sub>Mo<sub>6</sub>O<sub>31</sub>)<sub>2</sub>]·6H<sub>2</sub>O (**1**) and ((NHEPH<sub>2</sub>)<sub>2</sub>[Co<sup>II</sup>(H<sub>2</sub>O)<sub>6</sub>][P<sub>2</sub>Mo<sub>5</sub>O<sub>23</sub>]·2H<sub>2</sub>O (**2**) (NHEP = *N*-(2-hydroxyethyl)-piperazine), have been synthesized under hydrothermal conditions and characterized by elemental analyses, IR, TGA, single crystal X-ray diffraction and PXRD studies. In compound **1**, Ni(II) is sandwiched between two {P<sub>4</sub>Mo<sub>6</sub>O<sub>31</sub>}<sup>6-</sup> clusters and the residual negative charges are neutralized by NHEPH<sub>2</sub><sup>2+</sup>. In compound **2**, the [P<sub>2</sub>Mo<sub>5</sub>O<sub>23</sub>]<sup>6-</sup> ion exists as a discrete moiety and the negative charges are compensated by both [Co(H<sub>2</sub>O)<sub>6</sub>]<sup>2+</sup> and NHEPH<sub>2</sub><sup>2+</sup>. The extensive hydrogen bonding involving the organic cations and water molecules yielded three-dimensional (3D) open framework structures in these systems. These phosphomolybdate based compounds showed good catalytic efficiency in heterogeneous oxidation of styrene in the presence of an environmentally benign oxidant, H<sub>2</sub>O<sub>2</sub>, under mild conditions.

Received (in Montpellier, France)  
9th February 2016,  
Accepted 6th June 2016

DOI: 10.1039/c6nj00440g

www.rsc.org/njc

## Introduction

Polyoxometalates (POMs)<sup>1</sup> of early transition metal oxide clusters have attracted great interest in the solid-state materials chemistry, due to their structural and compositional diversity, and great potential toward applications in catalysis, sorption, ion exchange, optical, electro- and magnetic materials.<sup>2</sup> Recently, an intriguing area in this field has been the construction of organic–inorganic hybrid materials based on POMs. Several successful strategies have been developed to design such materials.<sup>3</sup> One of the promising methods is to connect POM building units with secondary transition metal complexes acting as inorganic bridging groups *via* covalent bonds under hydrothermal or solvothermal conditions. These reaction conditions help in increasing the solubility of inorganic and organic materials to form hybrid compounds. The transition metal complexes can dramatically influence the inorganic oxide microstructure. Therefore, one can combine the merit of POMs and transition metal complexes to constitute some interesting compounds with unique properties. Many examples have been explored recently,

including discrete clusters,<sup>4</sup> one-dimensional chains,<sup>5</sup> and two-,<sup>6</sup> and three-dimensional frameworks.<sup>7</sup>

Among the different POM clusters, phosphorus containing POMs constitute a remarkable family with diverse structures and applications. In all phosphomolybdates, the compounds constructed from {P<sub>4</sub>Mo<sub>6</sub>} and {P<sub>2</sub>Mo<sub>5</sub>} as the basic building units are structurally very diverse and have extensive application prospects. However, the design and synthesis of such compounds pose a challenge due to the following facts: (i) most of the syntheses involve one-pot reactions of negatively charged polyoxometalate clusters with positively charged cations or structure directing agents; and (ii) under such conditions difficulties arise as the reaction proceeds in a complex pathway. However, the charge balancing cations assume the major role in the assembly of the building blocks leading to the formation of the bulk material, which can be manipulated to tailor the assembly process.

Lately, the concept of secondary building units (SBUs) has been widely used by Yaghi, Williams, Kitagawa, and co-workers for understanding and predicting topologies of structures and it has been proved to be helpful in directing the construction of desired structures.<sup>8–13</sup> The basic building unit like {P<sub>4</sub>Mo<sub>6</sub>} can also be further assembled *via* a transition metal cation which is sandwiched between two P<sub>4</sub>Mo<sub>6</sub> units to form M<sup>n+</sup>[P<sub>4</sub>Mo<sub>6</sub>]<sub>2</sub><sup>(12-n)-</sup>.<sup>14</sup> Again, the construction of a simple metal–organic framework system can also be achieved by using simple transition metal cations and/or organic amine cations to balance the charge on the POM units. In this paper, we report two inorganic–organic hybrid materials formed from phosphomolybdates, namely

<sup>a</sup> Department of Chemistry Jadavpur University, Kolkata 700 032, India.

E-mail: mali@chemistry.jdvu.ac.in; Fax: +91-33-2414-6223

<sup>b</sup> Postgraduate Department of Chemistry, Panskura Banamali College, Panskura RS, Purba Medinipur, West Bengal 721 152, India

† Electronic supplementary information (ESI) available. CCDC 1431341 and 1431342. For ESI and crystallographic data in CIF or other electronic format see DOI: 10.1039/c6nj00440g

(NHEPH<sub>2</sub>)<sub>5</sub>[Ni<sup>II</sup>(P<sub>4</sub>Mo<sub>6</sub>O<sub>31</sub>)<sub>2</sub>].6H<sub>2</sub>O (**1**) and {(NHEPH<sub>2</sub>)<sub>2</sub>[Co<sup>II</sup>(H<sub>2</sub>O)<sub>6</sub>]}[P<sub>2</sub>Mo<sub>5</sub>O<sub>23</sub>].2H<sub>2</sub>O (**2**) (NHEPH<sub>2</sub><sup>2+</sup>, doubly protonated *N*-(2-hydroxyethyl)-piperazine) derived under hydrothermal conditions. The structure directing role of NHEPH<sub>2</sub><sup>2+</sup> is quite noteworthy as the heteroatom (O and N) donor sites not only participate in the charge compensation but are also involved in strong hydrogen bonding interactions resulting in the construction of 3D (three-dimensional) open network structures. Interestingly, compound **1** has a sandwiched structure in which the Ni(II) ion is trapped between two {P<sub>4</sub>Mo<sub>6</sub>O<sub>31</sub>}<sup>6-</sup> clusters, while in complex **2**, the Co(II) ion is present as a discrete [Co(H<sub>2</sub>O)<sub>6</sub>]<sup>2+</sup> complex cation, compensating the charge of phosphomolybdates, {P<sub>2</sub>Mo<sub>5</sub>O<sub>23</sub>}<sup>6-</sup>, together with the NHEPH<sub>2</sub><sup>2+</sup> cation. Efficient heterogeneous catalytic oxidation of styrene in the presence of an environmentally benign oxidant, H<sub>2</sub>O<sub>2</sub>, under mild conditions has also been investigated.

## Experimental section

### Materials and reagents

Chemicals Na<sub>2</sub>MoO<sub>4</sub>, Co(NO<sub>3</sub>)<sub>2</sub>.6H<sub>2</sub>O and NiCl<sub>2</sub>.6H<sub>2</sub>O, NaCl, H<sub>3</sub>PO<sub>4</sub> were obtained from Merck, India. *N*-(2-Hydroxyethyl)-piperazine was purchased from Riedel-de Haen. All these chemicals were of reagent grade and used as received. De-ionized water was used as the solvent.

### Physical measurements

Elemental analyses were carried out using a Perkin-Elmer 240 elemental analyzer. The FTIR spectra of the compounds were recorded using KBr pellets at ambient temperatures in the range 4000–400 cm<sup>-1</sup> on a Nicolet Magna IR 750 series-II FTIR spectrophotometer. Thermo gravimetric analyses (TGA) were performed on a Perkin-Elmer Pyris Diamond TGA/DTA analyzer in flowing N<sub>2</sub> at a heating rate of 12 °C min<sup>-1</sup>. The powder X-ray diffraction (PXRD) data were registered on a Bruker D8 Advance

X-ray diffractometer using Cu-K<sub>α</sub> radiation ( $\lambda = 1.5418 \text{ \AA}$ ) operating at 40 kV and 40 mA. The XRD patterns were recorded in the  $2\theta$  range of 3–50 using a LynxEye detector (1D mode) with a step size of 0.02 and a dwell time of 1 s per step.

### Single-crystal X-ray diffractions

Single-crystal X-ray data of complexes **1** and **2** were collected at 293 K on a Bruker SMART APEX-II CCD diffractometer using graphite monochromated Mo-K<sub>α</sub> radiation ( $\lambda = 0.71073 \text{ \AA}$ ). Data collection, reduction, structure solution, and refinement were performed using the Bruker APEX-II suite (v2.0-2) program. All available reflections to  $2\theta_{\text{max}}$  were harvested and corrected for Lorentz and polarization factors using Bruker SAINT plus.<sup>15</sup> Reflections were then corrected for absorption; inter-frame scaling, and other systematic errors using SADABS.<sup>16</sup> The structures were solved by direct methods and refined by means of full-matrix least-squares technique based on  $F^2$  using SHELX-97 software package.<sup>16</sup> During the refinement of **1** and **2**, non-hydrogen atoms were anisotropically refined; however, for a disordered cation NHEPH<sub>2</sub><sup>2+</sup> sitting on an inversion centre in compound **1** the ADP restraint was applied due to its unreasonable anisotropic  $U_{\text{eq}}$  parameters. All of the hydrogen atoms belonging to carbon atoms were placed in their geometrically idealized positions and were isotropically treated based on their respective parent atoms. Although the H atoms attached to heteroatoms in the NHEPH<sub>2</sub><sup>2+</sup> cation and water molecules were located in the difference Fourier maps in compound **2**, H atoms on water molecules in **1** cannot be found from the residual peaks and were just directly included into the final molecular formula, as the short O<sub>water</sub>...O<sub>POM</sub> and O<sub>water</sub>...O<sub>water</sub> distances (2.5–2.8 Å) implied the presence of extensive H-bonding interactions in the solid state in **1**. The drawings of molecules were generated using the DIAMOND-3.0 and Mercury 2.4 programs. The method of crystallographic data collection and structural detail are listed in Table 1.

Table 1 Crystallographic data and details of the structure determination

Formula	C <sub>30</sub> H <sub>64</sub> Mo <sub>12</sub> N <sub>10</sub> NiO <sub>73</sub> P <sub>8</sub>	C <sub>12</sub> H <sub>52</sub> CoMo <sub>5</sub> N <sub>4</sub> O <sub>35</sub> P <sub>2</sub>
Formula weight	3190.64	1413.15
Crystal system	Triclinic	Monoclinic
Space group	$P\bar{1}$ (no. 2)	$C2/c$ (no. 15)
$a$ [Å]	13.244(5)	9.7440(11)
$b$	13.546(5)	28.086(4)
$c$	14.691(5)	18.685(3)
$\alpha$ [°]	74.100(5)	90
$\beta$	69.748(5)	126.780(5)
$\gamma$	65.588(5)	90
$V$ [Å <sup>3</sup> ]	2225.0(14)	4095.6(12)
$Z$	1	4
$D(\text{calc.})$ [g cm <sup>-3</sup> ]	2.381	2.292
$\mu(\text{MoK}\alpha)$ [mm]	2.104	2.072
$F(000)$	1550	2796
Temperature (K)	293	293
Radiation [Å] MoK <sub>α</sub>	0.71073	0.71073
$\theta$ min–max [°]	1.5, 27.2	1.8, 32.6
Dataset	–16: 16; –17: 17; –18: 18	–42: 42; –14: 14; –27: 27
Tot., uniq. data, $R(\text{int})$	35 849, 9812, 0.028	29 665, 6300, 0.075
Observed data [ $I > 2.0 \sigma(I)$ ]	9188	4412
$N_{\text{ref}}, N_{\text{par}}$	9812, 630	6300, 311
$R, wR_2, S$	0.0318, 0.0912, 1.05	0.0619, 0.1545, 1.08
Min. and max. resd. dens. [e Å <sup>-3</sup> ]	–1.89, 2.27	–1.81, 2.41

## Syntheses of complexes

**(NHEPH<sub>2</sub>)<sub>5</sub>[Ni<sup>II</sup>(P<sub>4</sub>Mo<sub>6</sub>O<sub>31</sub>)<sub>2</sub>]-6H<sub>2</sub>O (1).** Na<sub>2</sub>MoO<sub>4</sub> (1.20 g, 5 mmol) was dissolved in 20 mL of 1.0 M NaCl solution. The pH was adjusted to 3.5 by adding 4.0 M nitric acid. The colourless solution was heated to 80 °C and stirred for 30 min. *N*-(2-Hydroxyethyl)piperazine (NHEP) (0.703 g, 5.4 mmol) and H<sub>3</sub>PO<sub>4</sub> (0.25 g, 2.55 mmol, 85%) were added slowly to the hot solution while stirring and the mixture became blue in colour. After 15 min, 5 mL aqueous solution of NiCl<sub>2</sub>·6H<sub>2</sub>O (0.427 g, 1.8 mmol) was added dropwise to obtain a brown heavy precipitate. Then, the entire mixture was transferred into a Teflon jacket in a PTFE-lined stainless steel pressure vessel and was kept in an oven at 160 °C for consecutive five days under autogenous pressure. The solution was cooled by decreasing the temperature at a regular interval of 5 °C for one day. After cooling the autoclave to room temperature, brown block shaped

crystals were obtained, filtered, washed several times with distilled water and dried in air. Yield, 32% (based on Mo). Elemental analysis: anal. calc. value for molecular formula, C<sub>30</sub>H<sub>64</sub>Mo<sub>12</sub>N<sub>10</sub>NiO<sub>73</sub>P<sub>8</sub> (M<sub>w</sub> = 3190.64): C, 11.29; H, 2.02; N, 4.39; found C, 11.34; H, 2.05; N, 4.46.

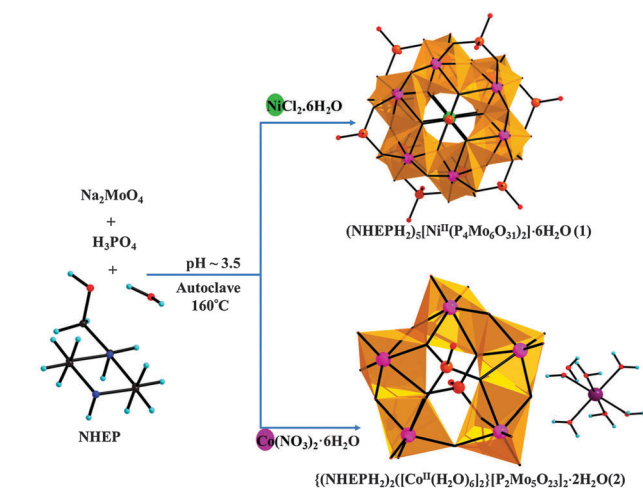
**{(NHEPH<sub>2</sub>)<sub>2</sub>[Co<sup>II</sup>(H<sub>2</sub>O)<sub>6</sub>]}[P<sub>2</sub>Mo<sub>5</sub>O<sub>23</sub>]-2H<sub>2</sub>O (2).** Compound 2 was prepared following a very similar procedure as described in **1** using Co(NO<sub>3</sub>)<sub>2</sub>·6H<sub>2</sub>O (0.308 g, 1.04 mmol) instead of NiCl<sub>2</sub>·6H<sub>2</sub>O. Deep pink block shaped crystals were obtained on cooling which were then filtered, washed several times with distilled water, and dried in air. Yield, 25% based on Mo. Elemental analysis: anal. calc. value for molecular formula, C<sub>12</sub>H<sub>52</sub>CoMo<sub>5</sub>N<sub>4</sub>O<sub>35</sub>P<sub>2</sub> (M<sub>w</sub> = 1413.15): C, 10.20; H, 3.71; N, 3.96; found C, 10.30; H, 3.41; N, 3.96.

## Results and discussion

Complexes **1** and **2** were synthesized by the reaction between Na<sub>2</sub>MoO<sub>4</sub> and appropriate metal ions (Ni<sup>II</sup> for complex **1** and Co<sup>II</sup> for complex **2**) in the presence of H<sub>3</sub>PO<sub>4</sub> and a structure directing agent like *N*-(2-hydroxyethyl)piperazine (NHEP) at pH ~ 3.5 under hydrothermal conditions (Scheme 1).

### Structural description of complexes **1** and **2**

The single crystal X-ray diffraction analysis shows that complex (NHEPH<sub>2</sub>)<sub>5</sub>[Ni<sup>II</sup>(P<sub>4</sub>Mo<sub>6</sub>O<sub>31</sub>)<sub>2</sub>]-6H<sub>2</sub>O (**1**) crystallized in the triclinic system with space group *P* $\bar{1}$ . The anionic part of complex **1** is composed of two {P<sub>4</sub>Mo<sub>6</sub>O<sub>31</sub>}<sup>6-</sup> clusters linked by the hexacoordinated Ni(II) ion in which the Ni centre is sandwiched between two {P<sub>4</sub>Mo<sub>6</sub>O<sub>31</sub>}<sup>6-</sup> units (Fig. 1a and d). Two wheel-like frameworks of {P<sub>4</sub>Mo<sub>6</sub>O<sub>31</sub>}<sup>6-</sup> units are connected by one Ni centre (Fig. 1b and e). The charge on the polyoxo anion is balanced by the presence of doubly protonated NHEPH<sub>2</sub><sup>2+</sup> cations in the asymmetric unit.



Scheme 1 The preparation scheme of complexes **1** and **2**.

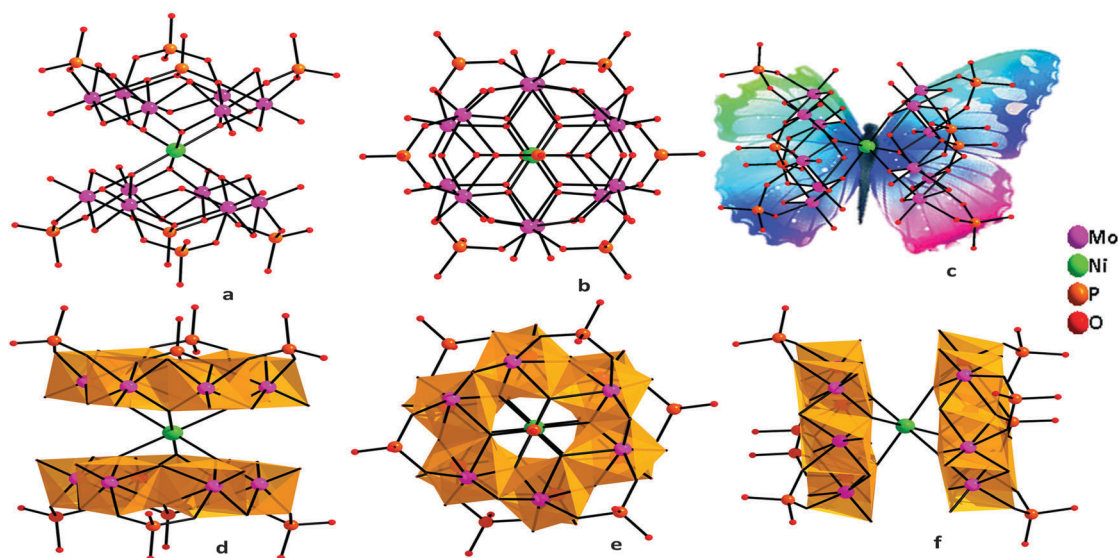


Fig. 1 The molecular view of complex **1** along the different crystallographic axes: *c* axis (a and d), *a* axis (b and e) and *b* axis (c and f), respectively. All counter ions and water molecules are omitted for clarity.

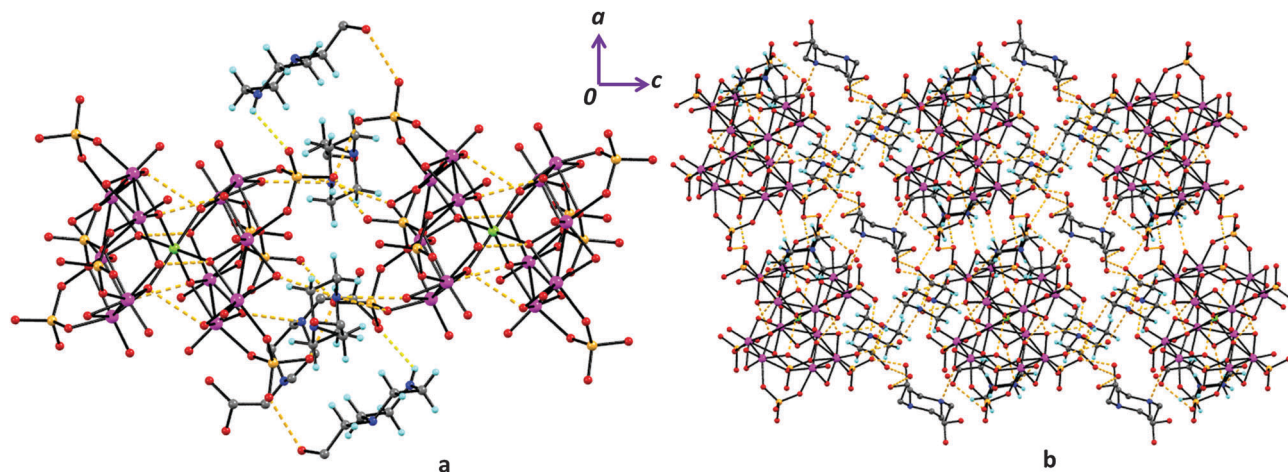


Fig. 2 (a) Type of H-bonding interactions involved in complex **1**; (b) the two dimensional (2D) supramolecular framework in the crystallographic *ac* plane.

As shown in Fig. 1, the  $[P_4Mo_6]$  cluster is constructed by six edge-sharing  $MoO_6$  octahedra and four  $PO_4$  tetrahedra with alternating three long  $Mo \cdots Mo$  contacts (avg. 3.485 Å) and three short  $Mo-Mo$  single bonds (avg. 2.594 Å). These three shorter  $Mo \cdots Mo$  contacts are supported by one oxygen atom externally and one oxygen atom internally which are directly connected to the Ni1 centre. Therefore, the central Ni(II) centre, located at a crystallographic inversion center, is octahedrally coordinated by six  $\mu_3O$  atoms from the two neighboring  $[P_4Mo_6]$  clusters. The Ni–O bond lengths lie in the range 2.141(3)–2.165(3) Å and O–Ni–O bond angles vary in the range 83.78(11)–180.00°, showing a distorted octahedron. Selected bond distances and bond angles are given in Table S1 (ESI<sup>†</sup>).

Out of four tetrahedral  $PO_4$  units, the central  $PO_4$  unit shares three  $\mu_3-O$  atoms with the six molybdenum atoms and three other  $PO_4$  groups share the corners with two  $MoO_6$  octahedra in which the central phosphate ion bridges the ring internally and each one of the other three phosphate groups bridges one long  $Mo \cdots Mo$  contact externally. Each P atom is in a tetrahedral environment surrounded by four oxygen atoms. Now, a closer inspection of the structure of complex **1** reveals the presence of a number of H-bonding interactions between the non-coordinated counter cation  $NHEPH_2^{2+}$  and the coordinated oxygen atoms (namely O5 and O30) with the Mo2 centre of the sandwich complex in a bifurcated fashion with  $N4-H4D \cdots O5 = 2.42(9)$  Å and  $N4-H4D \cdots O30 = 2.27(7)$  Å.

Again, the hydroxyl group (–OH) of this non-coordinated counter cation is involved in bifurcated H-bonding with the oxygen atom of one phosphate group (O20) ( $O32A \cdots O20 = 2.634$  Å) and a water molecule (O37) ( $O32A \cdots O37 = 2.845$  Å). Likewise, the other non-coordinated counter cation (O36) is bifurcated and hydrogen bonded with the oxygen atom of another phosphate group (O19) ( $O36 \cdots O19 = 2.727$  Å) and a water solvent (O37) ( $O36 \cdots O37 = 2.732$  Å) in the outer coordination sphere. As a consequence, O37 acts as a connector between two hydroxyl groups (–OH) of two counter cations through H-bonding interactions. Hence, these H-bonding interactions

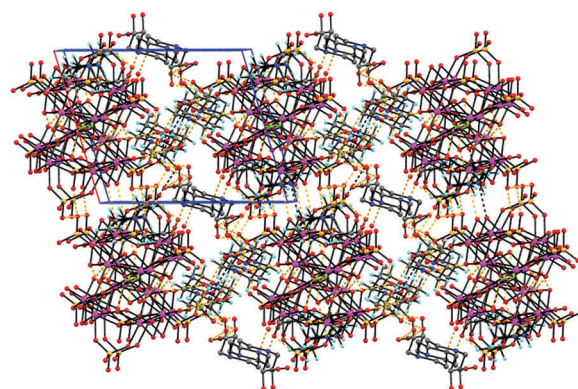


Fig. 3 The supra-molecular H-bonded 3D network along the crystallographic *b* axis.

are responsible for the extension of the structure of complex **1** into a 2D framework (Fig. 2) which is further extended to form a 3D network along the crystallographic *b* axis (Fig. 3). Now, some of the related H-bonding interactions formed in complex **1** by the non-coordinated water molecules (O35 and O34) in the asymmetric unit are given in Table S2 (ESI<sup>†</sup>).

The single crystal X-ray diffraction analysis reveals that complex **2** crystallizes in a triclinic system with space group  $C2/c$ . Compound **2** is based on the  $\{P_2Mo_5\}$  cluster. As it is usually observed that the  $\{P_2Mo_5\}$  cluster (see Fig. 4) can be viewed as two  $PO_4$  tetrahedra that cap, from either sides, an irregular ring of five distorted  $MoO_6$  octahedra, linked by one corner-shared and four edge-shared oxygen atoms. Each  $PO_4$  tetrahedron shares three oxo-groups with the  $MO_6$  octahedron. One of these oxo-groups adopts a  $\mu_2$ -bridging mode, linking one molybdenum site and the phosphorus atom and the other two adopt a  $\mu_3$ -bridging mode, linking two molybdenum and one phosphorus atoms and the other remain free from coordination. The two  $[Co(H_2O)_6]^{2+}$  ions, two water molecules (O32 and O33) and two  $NHEPH_2^{2+}$  cations, are also present in the asymmetric unit which balances the overall charge on  $\{P_2Mo_5O_{23}\}^{6-}$ . The organic

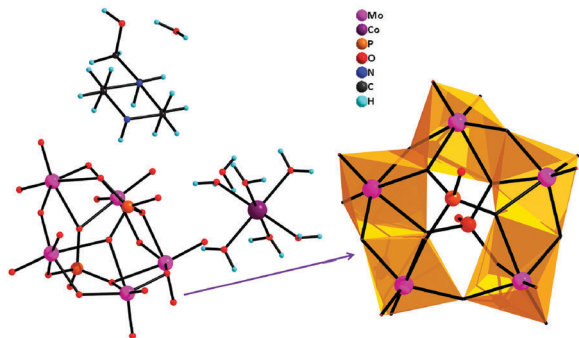


Fig. 4 The molecular view of complex **2** with a polyhedral representation.

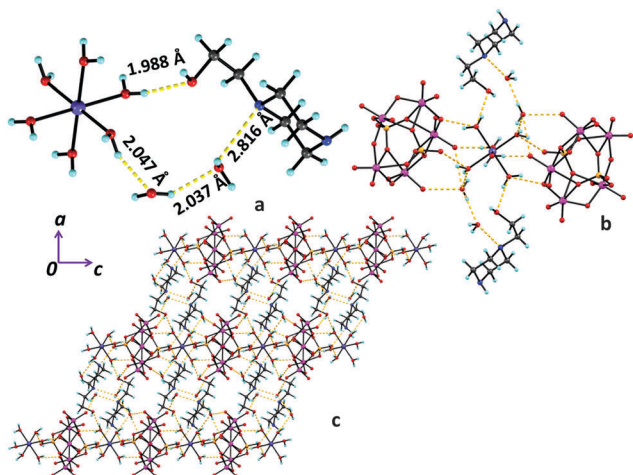


Fig. 5 (a) The  $[\text{Co}^{\text{II}}(\text{H}_2\text{O})_6]^{2+}$  involved in H-bonding with  $\text{NHEPH}_2^{2+}$  and water molecules; (b) the H-bonding pattern in complex **2**; (c) the H-bonded supramolecular 2D framework in the crystallographic  $ac$  plane.

cation  $\text{NHEPH}_2^{2+}$  has terminal N, O (N1, N2 and O30, O31) sites which make interaction with the water molecule of the  $[\text{Co}(\text{H}_2\text{O})_6]^{2+}$  ion and with the O-atom (O13) of the POM cluster. The free solvent water molecules also take part in hydrogen bonding with  $[\text{Co}(\text{H}_2\text{O})_6]^{2+}$  and the POM which are responsible for generating a 2D supramolecular structure (Fig. 5). This is further extended to form a 3D framework along the crystallographic  $b$  axis (Fig. S1, ESI<sup>†</sup>). The H-bonding interactions are given in Table S3 (ESI<sup>†</sup>).

### IR analysis

Complex **1** exhibits complex patterns of the IR spectrum with bands at  $506\text{--}961\text{ cm}^{-1}$  ascribed to  $\nu(\text{Mo}\text{--}\text{O})$  and  $\nu(\text{Mo}\text{--}\text{O}\text{--}\text{Mo})$ . The absorption bands at  $1009\text{ cm}^{-1}$  are assigned to  $\nu(\text{P}\text{--}\text{O})$ . A series of bands in the region  $1460\text{--}1751\text{ cm}^{-1}$  are characteristic of  $\text{NHEPH}_2^{2+}$ . The broad band at  $3435\text{ cm}^{-1}$  is ascribed to  $\text{H}_2\text{O}$  molecules. These results are in accordance with the structural findings. For complex **2**, two strong bands in the range  $690\text{--}920\text{ cm}^{-1}$  are associated with  $\nu_{\text{sym}}(\text{Mo}\text{=}\text{O})$  and  $\nu_{\text{asym}}(\text{Mo}\text{=}\text{O})$  and the medium to strong intensity band in the  $560\text{--}590\text{ cm}^{-1}$  region is attributed to  $\nu(\text{Mo}\text{--}\text{O}\text{--}\text{Mo})$ . A series of medium intensity bands in the  $1070\text{--}1747\text{ cm}^{-1}$  range are associated with  $\text{NHEPH}_2^{2+}$  cations, and the broad band at about

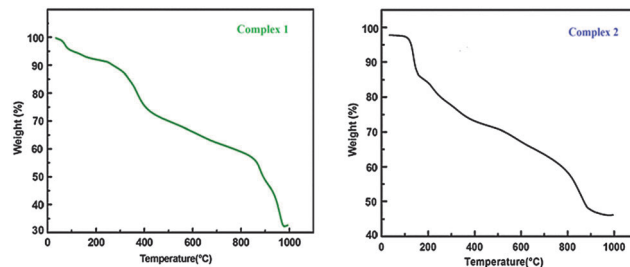


Fig. 6 (a) Thermo-gravimetric analysis of complex **1** and (b) of complex **2**.

$3212\text{ cm}^{-1}$  is associated with the water of crystallization.<sup>17</sup> The IR spectra are shown in Fig. S2(a) and (b) (ESI<sup>†</sup>).

### Thermo-gravimetric analysis

Thermal stability for compounds **1** and **2** were investigated by TGA. For both compounds, thermal decomposition proceeds *via* three steps with very similar profiles (Fig. 6a and b respectively). The initial endothermic mass loss below  $100\text{ }^\circ\text{C}$  for **1** corresponds to the release of six lattice  $\text{H}_2\text{O}$  molecules (calc. 9.66%; found 9.69%). Again, in the temperature range  $100\text{--}480\text{ }^\circ\text{C}$  mass loss corresponds to the decomposition of three  $\text{NHEPH}_2^{2+}$  molecules (calc. 8.42%; found 8.49%). The final mass loss is obtained above  $900\text{ }^\circ\text{C}$  for **1** may be due to complete rupture of the POM moiety into  $\text{P}_2\text{O}_5$  and  $\text{NiMoO}_4$  fragments. Again for complex **2** endothermic mass loss below  $200\text{ }^\circ\text{C}$  corresponds to the release of two lattice  $\text{H}_2\text{O}$  and six coordinated  $\text{H}_2\text{O}$  molecules (calc. 8.98%; found 9.30%). The resulting phase is thermally stable up to  $480\text{ }^\circ\text{C}$ . Again in the region  $486\text{--}800\text{ }^\circ\text{C}$  mass loss corresponds to the decomposition of two  $\text{NHEPH}_2$  molecules (calc. 7.12%; found 7.13%) from complex **2**. The final mass loss is obtained above  $800\text{ }^\circ\text{C}$  for **2** probably due to complete rupture of the POM moiety into  $\text{P}_2\text{O}_5$  and  $\text{MoO}_3$  fragments.

### Catalysis

A mixture of complex **1** (catalyst) (20 mg, 0.0063 mmol) and styrene (substrate) (0.5 g, 4.8 mmol) was dissolved in 10 mL MeCN solvent and the resulting solution was taken into a 50 mL two-necked round bottom flask, of which one neck was closed with a rubber septum and the other was fitted with a condenser. To the above solution was then added 1 mL of 30%  $\text{H}_2\text{O}_2$ . The resulting solution did not show any change in the colour. The solution was then heated in an oil bath to reflux for 24 h at  $60\text{ }^\circ\text{C}$ . No further addition of  $\text{H}_2\text{O}_2$  was done. The reaction was monitored thoroughly and it was found that the complex was not soluble in acetonitrile medium. So, the overall reaction mixture was heterogeneous and no ether extraction was needed for GC analysis. An aliquot (0.1 mL) of the reaction solution was withdrawn with the help of a long needle 10  $\mu\text{L}$  syringe and injected to the GC port. The same catalytic protocol was followed with complex **2** (20 mg, 0.0144 mmol) and it was also found to be heterogeneous for oxidation of styrene in acetonitrile medium. The results of oxidation are presented in Tables 2 and 3.

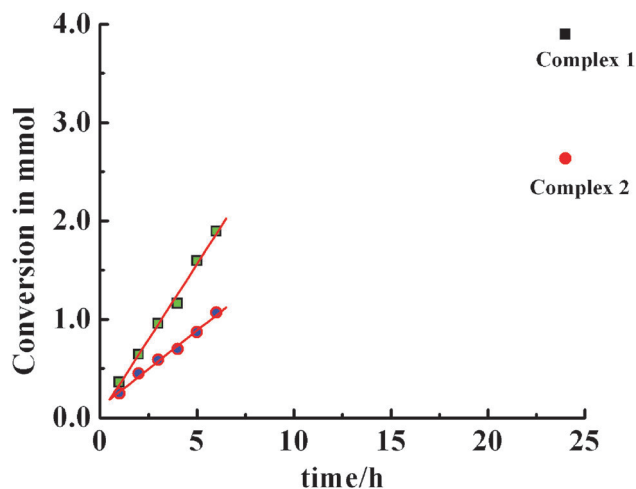
In the case of Ni-POM (catalyst **1**), the total conversion of styrene after 24 h was 81.14% with benzaldehyde selectivity of 84.47%.

**Table 2** Heterogeneous catalytic oxidation of styrene catalysed by complex **1** in MeCN (temperature = 60 °C)

Time (h)	Total conversion of styrene	Benzaldehyde	Styrene oxide	Benzoic acid
1	7.521	89.009	5.02	1.02
2	13.4036	77.35	6.57	8.9
3	19.96	79.96	5.46	8.743
4	24.187	79.46	4.702	9.56
5	33.25	79.99	4.73	9.138
6	39.45	81.58	3.97	3.67
24	81.141	84.47	1.813	7.39

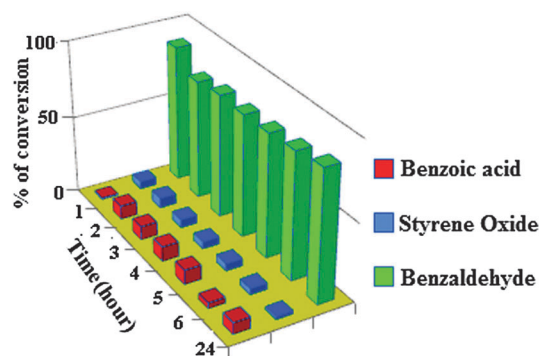
**Table 3** Heterogeneous catalytic oxidation of styrene catalysed by complex **2** in MeCN (temperature = 60 °C)

Time (h)	Total conversion of styrene	Benzaldehyde	Styrene oxide	Benzoic acid
1	5.14	92.46	6.423	1.14
2	9.34	84.91	10.82	5.86
3	12.24	83.53	9.24	7.24
4	14.498	85.97	7.56	6.44
5	18.075	85.58	7.714	6.69
6	22.23	85.89	5.26	8.8
24	54.85	89.148	3.249	7.58

**Fig. 7** A plot of conversion of styrene (mmol) as a function of time (h) for complexes **1** and **2**.

In the case of Co-POM (catalyst **2**), after 24 h reaction the total conversion was 54.85% with high benzaldehyde selectivity, *i.e.*, 89.15%. A plot of conversion of styrene (in mmol) as a function of time (in h) is shown in Fig. 7. Linear fits of these time based conversions up to 6 h give  $k_{\text{obs}}(1) = 0.31 \text{ mmol h}^{-1}$  and  $k_{\text{obs}}(2) = 0.15 \text{ mmol h}^{-1}$  for complexes **1** and **2**, respectively.

Table 4 represents a comparison of the catalytic activities of our catalysts with other POM-based catalysts reported for styrene oxidation. It is found that phosphomolybdate containing metal-salen complexes under homogeneous catalytic conditions in the presence of 30%  $\text{H}_2\text{O}_2$ <sup>18-20</sup> as oxidants led to ~80% conversion of styrene with 80-90% benzaldehyde selectivity, whereas Co-POM complexes showed very poor conversion (4-17%). Also, M-PMo<sub>11</sub> based POMs (M = Co and Ni) also showed poor percentage of conversion of styrene under solvent-free heterogeneous conditions.<sup>21</sup> On the other hand, our complexes showed better conversion and comparable benzaldehyde selectivity when compared with other POM based heterogeneous catalysts as described in Table 4. To check the catalytic efficacy of our POM complexes we have run the blank reactions taking only ( $\text{H}_2\text{O}_2 + \text{styrene} + \text{MeCN}$ ), where only 0.26% conversion was noted in 6 h. Again, when the above reaction was carried out in the presence of either  $\text{Co}(\text{NO}_3)_2$  or  $\text{NiCl}_2$ , the % conversion of styrene was found to be only ~5% thereby clearly indicating the catalytic properties of our Co-POM and Ni-POM complexes. A brief summation of

**Fig. 8** Catalytic conversion of styrene to benzaldehyde/styrene oxide formation with respect to time for complex **1**.**Table 4** Comparison of the catalytic activities of different POM-based catalysts for styrene oxidation

Catalyst	Solvent	Temp (°C)	Oxidant	% Conversion	% Selectivity benzaldehyde	Catalytic nature	Ref.
Ni(salen)-POM	CH <sub>3</sub> CN	60	H <sub>2</sub> O <sub>2</sub>	79	97.53	Homogeneous	18
Co(salen)-POM	CH <sub>3</sub> CN	60	H <sub>2</sub> O <sub>2</sub>	85	81	Homogeneous	19
Co-POM <sup>a</sup>	CH <sub>3</sub> CN	60	H <sub>2</sub> O <sub>2</sub>	14.1	86.2	Homogeneous	20
Co-POM <sup>b</sup>	CH <sub>3</sub> CN	60	H <sub>2</sub> O <sub>2</sub>	16.7	81.4	Homogeneous	20
Co-POM <sup>c</sup>	CH <sub>3</sub> CN	60	H <sub>2</sub> O <sub>2</sub>	2.2	72.0	Homogeneous	20
Co-POM <sup>d</sup>	CH <sub>3</sub> CN	60	H <sub>2</sub> O <sub>2</sub>	3.8	76.2	Homogeneous	20
PMo <sub>11</sub> Co	Solvent free	80	TBHP	41.1	92.2	Heterogeneous	21
PMo <sub>11</sub> Ni	Solvent free	80	TBHP	39.9	87.2	Heterogeneous	21
Ni-POM	CH <sub>3</sub> CN	60	H <sub>2</sub> O <sub>2</sub>	81.14	84.47	Heterogeneous	Present work
Co-POM	CH <sub>3</sub> CN	60	H <sub>2</sub> O <sub>2</sub>	54.85	89.15	Heterogeneous	Present work

<sup>a</sup>  $(\text{H}_4\text{TETA})_2[(\text{Co}^{\text{II}}\text{TREN})_2\text{Co}^{\text{II}}\text{Mo}^{\text{V}}_{12}\text{P}_8\text{O}_{52}(\text{OH})_{10}] \cdot 4\text{H}_2\text{O}$  (TREN = tris(2-aminoethyl)amine). <sup>b</sup>  $(\text{H}_4\text{TETA})_2(\text{C}_6\text{H}_{18}\text{N}_3)_2[\text{Co}^{\text{II}}\text{Mo}^{\text{V}}_{12}\text{P}_8\text{O}_{54}(\text{OH})_8] \cdot 5\text{H}_2\text{O}$  ( $\text{C}_6\text{H}_{15}\text{N}_3 = N$ -(2-aminoethyl)piperazine), TETA = triethylenetetramine. <sup>c</sup>  $[\text{H}_4\text{TREN}]_4[\text{Co}^{\text{II}}\text{Mo}^{\text{V}}_{12}\text{P}_8\text{O}_{56}(\text{OH})_6] \cdot 4\text{H}_2\text{O}$ . <sup>d</sup>  $[\text{H}_4\text{TETA}]_2[\text{Co}^{\text{II}}\text{Mo}^{\text{V}}_{12}\text{P}_8\text{O}_{48}(\text{OH})_{14}] \cdot 4\text{H}_2\text{O}$ .

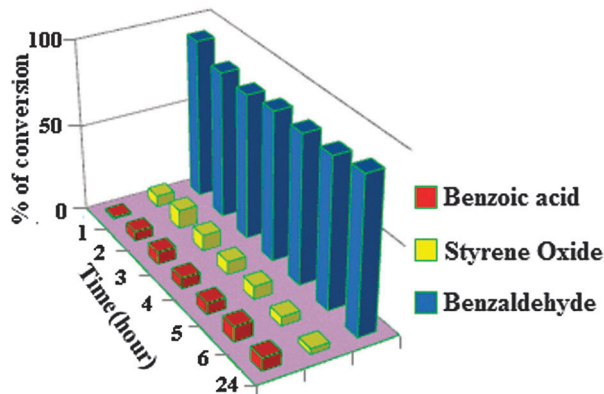


Fig. 9 Catalytic conversion of styrene to benzaldehyde/styrene oxide formation with respect to time for complex 2.

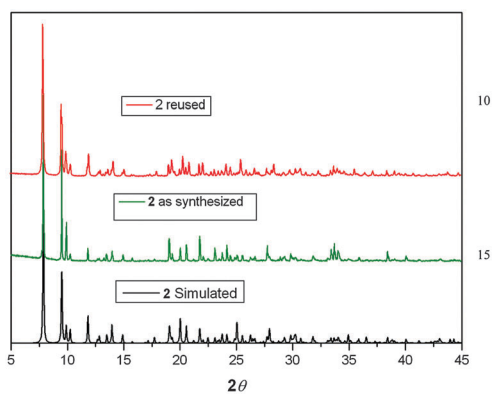


Fig. 10 Powder XRD plots of complex 2.

the results of the catalysis by complex 1 and complex 2 is incorporated in Table S4 (ESI<sup>†</sup>).

The selectivities of different products formed at different time intervals are graphically presented in Fig. 8 and 9. The catalytic oxidative conversion of styrene to benzaldehyde and other minor product formation as a function of time are shown in Fig. S3 and S4 (ESI<sup>†</sup>).

Both the complexes are heterogeneous in nature and it is proved by PXRD (Fig. 10 and Fig. S5, ESI<sup>†</sup>) and IR studies of the fresh and reused catalysts (after three consecutive uses) which showed very similar patterns (Fig. S6(a) and (b), ESI<sup>†</sup>).

## Conclusion

Two new phosphomolybdate based hybrid compounds (NHEPH<sub>2</sub>)<sub>5</sub>–[Ni<sup>II</sup>(P<sub>4</sub>Mo<sub>6</sub>O<sub>31</sub>)<sub>2</sub>]·6H<sub>2</sub>O (1) and {(NHEPH<sub>2</sub>)<sub>2</sub>–[Co<sup>II</sup>(H<sub>2</sub>O)<sub>6</sub>]}[P<sub>2</sub>Mo<sub>5</sub>O<sub>23</sub>]·2H<sub>2</sub>O (2) were synthesized under hydrothermal conditions and characterized by elemental analyses, IR, TG-DTA, and single-crystal X-ray diffraction and PXRD techniques. In compound 1, Ni(II) is sandwiched between two {P<sub>4</sub>Mo<sub>6</sub>O<sub>31</sub>}<sup>6–</sup> clusters whereas, in compound 2, the {P<sub>2</sub>Mo<sub>5</sub>O<sub>23</sub>}<sup>6–</sup> ion is present as a discrete moiety and the negative charges are compensated by both [Co(H<sub>2</sub>O)<sub>6</sub>]<sup>2+</sup> and NHEPH<sub>2</sub><sup>2+</sup>. Both the compounds are efficient for heterogeneous

catalytic oxidation of styrene in the presence of an environmentally benign oxidant H<sub>2</sub>O<sub>2</sub> under mild conditions leading to benzaldehyde with more than 80% selectivity.

## Acknowledgements

Financial support from DST, West Bengal, is gratefully acknowledged. L. P. and M. D. thank UGC (NET), New Delhi, for SRF fellowship.

## References

- M. T. Pope, *Heteropoly and Isopoly Oxometalates*, Springer, Berlin, 1983.
- Special issue on polyoxometalates: (a) C. Hill, *Guest Ed.*, 1998, **98**, 1, and references therein; (b) M. T. Pope and A. Müller, *Angew. Chem., Int. Ed. Engl.*, 1991, **30**, 30.
- (a) P. J. Hagrman, D. Hagrman and J. Zubieta, *Angew. Chem., Int. Ed. Engl.*, 1999, **38**, 2638; (b) D. Hagrman, P. Hagrman and J. Zubieta, *Inorg. Chim. Acta*, 2000, **212**, 300; (c) R. S. Rarig, R. Lam, P. Y. Zavalij, J. K. Ngala, R. L. LaDuca, J. E. Greedan and J. Zubieta, *Inorg. Chem.*, 2002, **41**, 2124; (d) L. Lisnard, A. Delbecq, P. Mialane, J. Marrot, E. Codjovi and F. Sécheresse, *J. Chem. Soc., Dalton Trans.*, 2005, 3913; (e) G. Hu, Y. Dong, X. He, H. Miao, S. Zhou and Y. Xu, *Inorg. Chem. Commun.*, 2015, **60**, 33.
- (a) L. Chen, Y. Wang, C. Hu, L. Feng, E. Wang, N. Hu, H. Jia, J. Sol, M. Yuan, Y. Li, E. Wang, C. Tian, L. Wang and C. Hu, *Inorg. Chem.*, 2003, **42**, 3670.
- (a) E. Burkholder, V. Golub, C. J. O'Connor and J. Zubieta, *Inorg. Chem. Commun.*, 2004, **7**, 363; (b) Y. Lu, Y. Xu, E. Wang, J. Lu, C. Hu and L. Xu, *Cryst. Growth Des.*, 2005, **5**, 257; (c) E. Burkholder, N. G. Armatas, V. Golub, C. J. O'Connor and J. Zubieta, *J. Solid State Chem.*, 2005, **178**, 3145.
- (a) Y. Li, G. De, M. Yuan, E. Wang, R. Huang, C. Hu, N. Hu and H. Jia, *J. Chem. Soc., Dalton Trans.*, 2003, 331; (b) M. Yuan, E. Wang, Y. Lu, Y. Li, C. Hu, N. Hu and H. Jia, *J. Solid State Chem.*, 2003, **170**, 192; (c) R. L. LaDuca, M. Desiak, R. S. Rarig and J. Zubieta, *Inorg. Chim. Acta*, 2002, **332**, 79.
- (a) P. J. Hagrman, C. Bridges, J. E. Greedan and J. Zubieta, *J. Chem. Soc., Dalton Trans.*, 1999, 2901; (b) D. G. Allis, R. S. Raig, E. Burkholder and J. Zubieta, *J. Mol. Struct.*, 2004, **688**, 11.
- H. L. Li, M. Eddaoudi, M. O'Keeffe and O. M. Yaghi, *Nature*, 1999, **402**, 276.
- N. L. Rosi, J. Eckert, M. Eddaoudi, D. T. Vodak, J. Kim, M. O'Keeffe and O. M. Yaghi, *Science*, 2003, **300**, 1127.
- R. Kitaura, K. Seki, G. Akiyama and S. Kitagawa, *Angew. Chem., Int. Ed.*, 2003, **42**, 428.
- S. S. Y. Chui, S. M. F. Lo, J. P. H. Charmant, A. G. Orpen and D. Williams, *Science*, 1999, **283**, 1148.
- S. M. F. Lo, S. S. Y. Chui, L. Y. Shek, Z. Y. Lin, X. X. Zhang, G. H. Wen and I. D. Williams, *J. Am. Chem. Soc.*, 2000, **122**, 6293.

- 13 (a) P. J. Hagrman, D. Hagrman and J. Zubieta, *Angew. Chem., Int. Ed.*, 1999, **38**, 2638; (b) X. H. Bu, W. Chen, S. L. Lu, R. H. Zhang, D. Z. Liao, W. M. Bu, M. Shionoya, F. Brisse and J. Ribas, *Angew. Chem., Int. Ed.*, 2001, **40**, 3201.
- 14 (a) Z. Hao, Q. Dong, L. Zhang, Y. Zhang and F. Luo, *CrystEngComm*, 2010, **12**, 977; (b) H. J. Jin, B. B. Zhou, Y. Yu, Z. F. Zhao and Z. H. Su, *CrystEngComm*, 2011, **13**, 585.
- 15 A. Altomare, M. C. Burla, M. Camalli, G. L. Casciarano, C. Giacovazzo, A. Guagliardi, A. G. G. Moliterni, G. Polidori and R. Spagna, *J. Appl. Crystallogr.*, 1999, **32**, 115.
- 16 G. M. Sheldrick, *Acta Crystallogr.*, 2008, **A64**, 112.
- 17 X. Lu, X. Wang, P. Li, X. Pei and C. Ye, *J. Mol. Struct.*, 2008, **872**, 129.
- 18 V. Mirkhani, M. Moghadam, S. Tangestaninejad, I. M. Baltork, E. Shams and N. Rasouli, *Appl. Catal., A*, 2008, **334**, 106.
- 19 V. Mirkhani, M. Moghadam, S. Tangestaninejad, I. M. Baltork and N. Rasouli, *Catal. Commun.*, 2008, **9**, 219.
- 20 Q. Chen, Y. Cui, Q. Sun, W. Pan, Q. Chen and Y. Xu, *Z. Anorg. Allg. Chem.*, 2009, **635**, 2302.
- 21 S. Pathan and A. Patel, *Catal. Sci. Technol.*, 2014, **4**, 648.